Frequency stabilization of DFB laser diodes at 1572 nm for spaceborne lidar measurements of CO_2

Kenji Numata,[1,2,*] Jeffrey R. Chen,[2] Stewart T. Wu,[2] James B. Abshire,[2] and Michael A. Krainak[2]

[1]*Department of Astronomy, University of Maryland, College Park, Maryland, 20742, USA*

[2]*NASA Goddard Space Flight Center, Greenbelt, Maryland, 20771, USA*

[*]*Corresponding author: kenji.numata@nasa.gov*

We report a fiber-based, pulsed laser seeder system that rapidly switches among 6 wavelengths across atmospheric carbon dioxide (CO_2) absorption line near 1572.3 nm for measurements of global CO_2 mixing ratios to 1-ppmv precision. One master DFB laser diode has been frequency-locked to the CO_2 line center using a frequency modulation technique, suppressing its peak-to-peak frequency drifts to 0.3 MHz at 0.8 sec averaging time over 72 hours. Four online DFB laser diodes have been offset-locked to the master laser using phase locked loops, with virtually the same sub-MHz absolute accuracy. The 6 lasers were externally modulated and then combined to produce the measurement pulse train.

OCIS codes 350.6090, 300.6380, 140.3425, 280.1910.

1. Introduction

CO_2 measurements from ice cores show that atmospheric CO_2 concentrations are higher now than they have been in the past 420,000 years [1]. It is becoming increasingly important to understand the nature and processes of the CO_2 sources and sinks, on a global scale, in order to make predictions of future atmospheric composition. Global measurements of the CO_2 mixing ratios from Earth orbit with 1-ppmv precision in the total column, 300-km spatial and monthly temporal resolution are needed to infer regional CO_2 terrestrial and oceanic sources and sinks in the presence of ~5-ppmv seasonal fluctuation [2-4]. The recent US National Research Council Decadal Survey for Earth Science [5] has recommended addressing these needs in a laser-based NASA mission – the Active Sensing of CO_2 Emissions over Nights, Days, and Seasons (ASCENDS). Spaceborne measurements are required for the global coverage and spatial resolution that go beyond the capability of ground-based measurement technologies [6]. Using the reflected sunlight as the light source, passive spaceborne instruments [7, 8] preclude measurements at nights and also suffer from various biases. Unlike the passive instruments, the active laser sounding approach for ASCENDS allows measurements of atmospheric CO_2 distributions with greater precision and spatial resolutions, over days and nights with global coverage.

A laser sounder for ASCENDS is currently under development at NASA Goddard. This instrument employs a nadir-viewing, differential-absorption lidar (DIAL) technique to measure CO_2 content in the atmospheric column using direct photon-counting detection of echo pulses from the surface of the earth [9]. As a part of this effort, the present work addresses the laser seeder system in the CO_2 transmitter for this instrument.

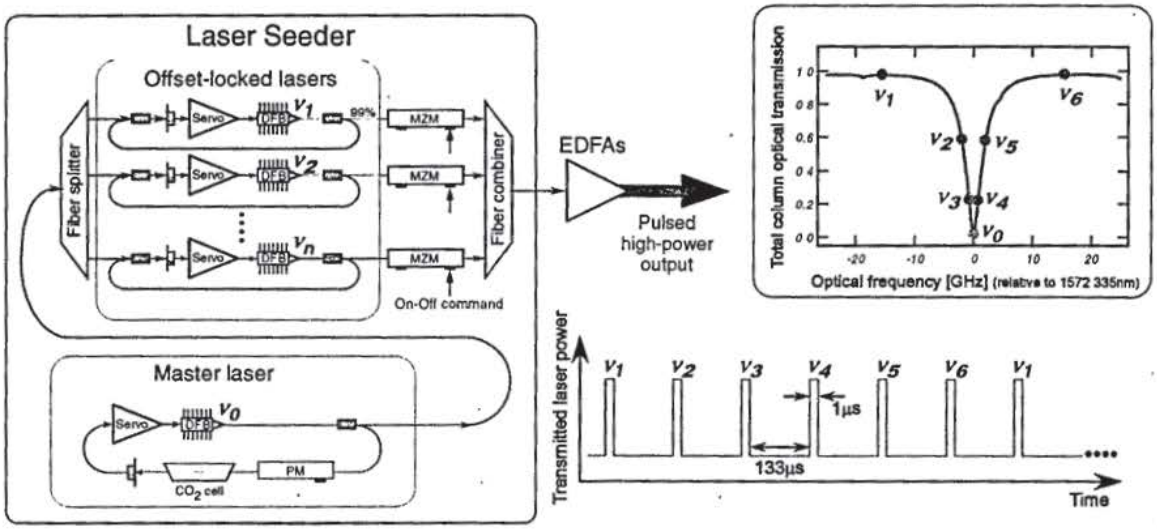

Fig. 1. Basic design concept for our CO_2 sounder transmitter. The laser seeder (*left*) is rapidly pulsed and switched among the 6 measurement laser frequencies to provide the wavelength-stepped pulse train (*lower right*) that is subsequently amplified by Erbium doped fiber amplifiers (EDFAs). The amplified pulse-train is used to repeatedly measure at 6 points across the 1572.335 nm CO_2 absorption line (*upper right*).

The basic design concept for our CO_2 sounder transmitter is illustrated in Fig. 1. Serving as the master oscillator, the laser seeder (Fig.1, *left*) defines spectral and temporal characteristics of the CO_2 transmitter. The seeder is rapidly pulsed and switched among the 6 measurement wavelengths to provide the wavelength-stepped pulse train that is subsequently amplified by Erbium doped fiber amplifiers (EDFAs). Since laser polarization drifts may cause undesirable amplitude fluctuations in the measurements, all components along the optical train were polarization maintaining (PM). A CO_2 line near 1572.335 nm was chosen for the measurement because of its adequate absorption strength, small temperature sensitivity, and minimum interference from other species [10]. Since CO_2 has diurnal, vertical transport, ideally the CO_2 measurement is uniformly sensitive to concentrations in the lower troposphere. This can be achieved by sampling the sides of the line where the absorption is pressure-broadened in the lower atmosphere. We used 6 measurement wavelengths, two offline and four on the sides of the

line, to allow us to model and correct for environmental and instrumental errors. The two-way transmittance of the 1572.335-nm CO_2 line from the 550-km orbit, as shown in Fig.1 (*upper right*), has a linewidth as narrow as ~3.3 GHz full width at half maximum and steep slopes on the sides, making the measurements sensitive to laser frequency drifts and uncertainties, as well as to CO_2 concentration. We wish to reduce the error contribution from the laser frequency to a small fraction of the total error budget, to allow more margins for other error sources. To ensure 1-ppmv precision for CO_2 measurements near 1572 nm, an error budget of 0.08 % is derived from an analysis of the sources of systematic errors, and a laser frequency stability as high as ± 0.3 MHz is required to meet the target error bound [11]. The CO_2 laser sounder measurements are most sensitive to slow frequency drifts, but insensitive to fast frequency noise because of the long pulse duration (~1 μsec) and the even longer photon counting average time (~10 sec). The present work focuses on suppressing slow laser frequency drifts (below 1 MHz) to meet the stringent ASCENDS requirement.

The laser seeder for CO_2 falls into the telecom L-band, allowing us to exploit advances in technologies driven by the telecom industry. The leverage of this highly reliable and rapidly improving technology provides high performance and cost efficiency. We chose distributed-feedback laser diodes (DFB-LDs) as our laser oscillators to take advantage of their proven reliability. Rather than locking lasers directly to the side slopes of the absorption line, we employed an offset locking technique to tune slave lasers precisely to desired optical frequencies, up to ±7 GHz away from that of a "master" laser. To do this, we have locked a master DFB-LD to 1572.335 nm CO_2 absorption line center (ν_0 in Fig. 1) and suppressed the peak-to-peak optical frequency drift to 0.3 MHz, better than the ASCENDS requirement. We further offset-locked four online DFB-LDs on the sides of the CO_2 line (ν_2 to ν_5 in Fig. 1), with virtually the same sub-

MHz precision in their absolute frequencies. The two offline DFB-LDs (ν_1 and ν_6) can tolerate much more frequency drifts and thus were left to free run under stabilized temperatures and currents. The 6 DFB-LDs were externally modulated to generate the pulses and subsequently combined to produce the measurement pulse train as shown in Fig. 1 (*lower right*). The pulses in this combined output were ~1 μsec wide separated by ~133 μsec. This off interval permits the pulses to completely clear the bottom 20 km of the atmosphere, which eliminated any crosstalk from cloud scattering. To suppress the crosstalk among the 6 wavelengths to < -32 dB, each modulator needs to have > 40 dB on/off extinction ratio (ER). This requirement was achieved with auto-biased telecom lithium-niobate (LN) Mach-Zehnder modulators (MZMs), to take advantage of their high reliability, compact size, and low power consumption. Based on these laser frequency locking and pulse modulation techniques, we have constructed a laser seeder for the CO_2 transmitter. Next, we present details on these techniques implemented for ground and airborne demonstrations, and show results of our laser seeder development work.

2. Absolute frequency locking

A. Absolute locking design considerations

It is difficult to suppress the slow frequency drift to sub-MHz by locking a laser frequency to an optical cavity. A molecular or atomic transition is thus preferred as the wavelength reference. Unfortunately, the well-known wavelength references for 1.5 μm lasers, such as $^{12}C_2H_2$ [12], $^{13}C_2H_2$ [13], $H^{13}C^{14}N$ [14], and ^{87}Rb [15], do not have any strong absorption lines near the 1572.335-nm CO_2 line selected for the measurement. Consequently, the 1572.335-nm CO_2 line itself becomes the reference of choice for the absolute wavelength locking.

Frequency locking of DFB-LDs to one side of a CO_2 line near 1573 nm within 5 MHz (rms) was reported using a 36-m multipass CO_2 cell [16]. Wavelength modulation (WM) technique has also been widely used to lock laser diode frequency to absorption peaks. In the WM technique, the laser frequency is dithered at an audio frequency by applying a small sinusoidal modulation on the injection current. To minimize undesirable wavelength and amplitude modulations in the laser output, the modulation depth need to be kept rather small, resulting in inferior signal-to-noise ratio (S/N) [17]. To achieve much better frequency stability, we adopted a frequency modulation (FM) spectroscopic technique [18, 19] to lock the master laser frequency to the 1572.335-nm CO_2 line center. Similar to the well-known Pound-Drever-Hall technique [20], this FM technique uses the external phase modulation and phase-sensitive detection at an RF frequency to generate a frequency discriminating error signal.

The predominant noise source with this FM technique is the time-varying residual amplitude modulation (RAM) arising from multi-path interference (MPI), polarization misalignment, and other sources, particularly in the phase modulator [21, 22]. Consequently, it is crucial to minimize the RAM in the phase modulator and the gas cell. In an earlier work, the same FM technique had been employed to lock a DFB-LD to a 10-cm-long $^{12}C_2H_2$ cell near 1527 nm using a bulk electro-optic (EO) phase modulator [23]. Bulk EO phase modulators were selected against wave-guided LN phase modulators due to the much higher RAM encountered in the latter. The telecom LN modulator technology has since been improved. We have selected compact telecom LN phase modulators for the present work to avoid the complexity of using free-space bulk components and high-voltage RF sources to drive EO modulators. The RAM in the LN phase modulators has been reduced to < 0.04-% peak-to-peak, low enough for our sub-MHz frequency stability requirement.

The same FM technique had also been used to lock lasers to CO_2 absorption lines near 2 μm, again using bulk EO phase modulators [24, 25]. The present work is more challenging because our CO_2 reference line is 10 times weaker than the CO_2 lines near 2 μm, an over 600 times weaker than the $^{12}C_2H_2$ lines near 1530 nm. Consequently, a much longer gas-cell path-length is required for our reference CO_2 cell.

B. Absolute locking setup

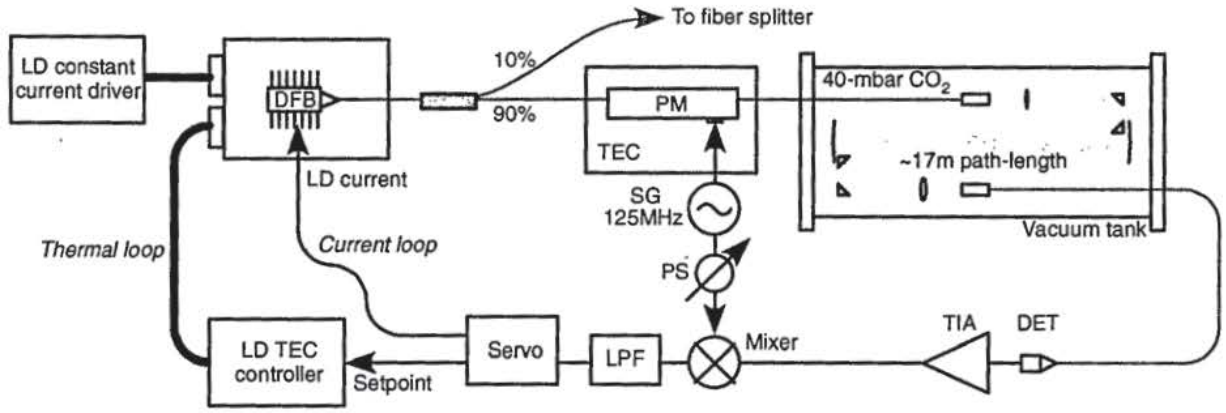

Fig. 2. Absolute frequency locking setup for the master DFB-LD: PM – phase modulator; DET – PIN detector; TIA – transimpedance amplifier; PS – phase shifter; SG – signal generator; LPF – low-pass filter.

Our absolute locking system is shown in Fig. 2. The master laser was a 40-mW single-mode (SM) PM DFB-LD with a narrow linewidth < 2 MHz (FRL15DCWD-A81-19070-B, OFS Fitel, LLC). It contains a built-in isolator with > 35 dB isolation to prevent unwanted feedbacks. The master laser output was split into two ways using a PM fiber coupler. 90 % of the light was used to lock this master laser. The rest is used to offset-lock slave DFB-LDs after being further split through a PM fiber splitter (discussed later). The 90-% laser output was passed through a fiber-coupled wave-guided 10-GHz LN phase modulator (PM-150-100-1-1-C2-I2-O2 APE, JDSU

Corp.). To further reduce error signal drift due to the RAM, the case temperature of this LN phase modulator was stabilized with a thermoelectric cooler (TEC). The modulated laser beam was subsequently passed through a CO_2 absorption cell with a path length of 17-m and CO_2 pressure of 40 mbar. The phase modulator was driven by a 125 MHz sinusoidal voltage at a modulation index of ~2.5, generating sidebands 125 MHz apart around the optical carrier. Unlike the case in WM technique, these sidebands ride on the steepest portions of the absorption line to allow much greater S/N. The transmitted laser beam was finally detected by a fiber-coupled InGaAs PIN photodiode. The detector current was AC-coupled to and amplified by a low-noise transimpedance amplifier (TIA). A demodulation circuit (comprising a mixer, a phase shifter, and a low-pass filter) makes phase sensitive detection of the amplified beatnote at 125 MHz and produces an error signal proportional to the laser frequency deviation from the CO_2 line center. The loop servo fed two signals back to the DFB-LD to stabilize its optical frequency: one slowly adapts the DFB-LD temperature through the TEC controller; the other rapidly adjusts the injection current through a resistor network [26] that adds the feedback on top of the constant bias current. The servo was controlled by an on-board microprocessor, which automatically finds the absorption peak and triggers switches in the servo circuit. Two identical absolute locking systems were built, and beatnote between the two independent lasers was used to measure the laser frequency noise.

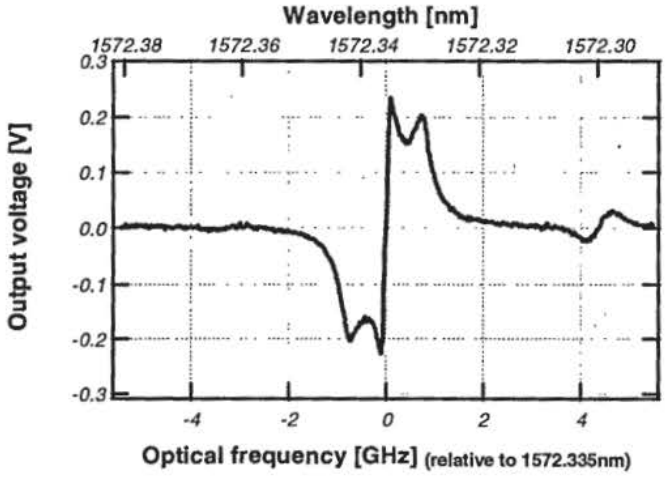

Fig. 3. The error signal measured in the absolute frequency locking setup shown in Fig. 2. The depression at the positive and negative peaks of the error signal is attributed to the mixer saturation.

Our CO_2 cell was carefully designed to minimize the MPI. Two spherical mirrors were placed inside a CO_2 chamber, forming a multi-pass optical delay line [27] with beam spots well separated on the mirrors. The laser beam was coupled in and out of the chamber through SM fibers hermetically sealed to the chamber, eliminating optical windows that could cause MPI. The high reflectivity of the protected-silver coated mirrors resulted in a low cell insertion loss of ~5 dB (gas absorption excluded). The CO_2 cell pressure, modulation frequency and depth, and the phase shifter delay were optimized to maximize the slope of the error signal shown in Fig. 3.

C. DFB-LD Frequency tuning transfer function

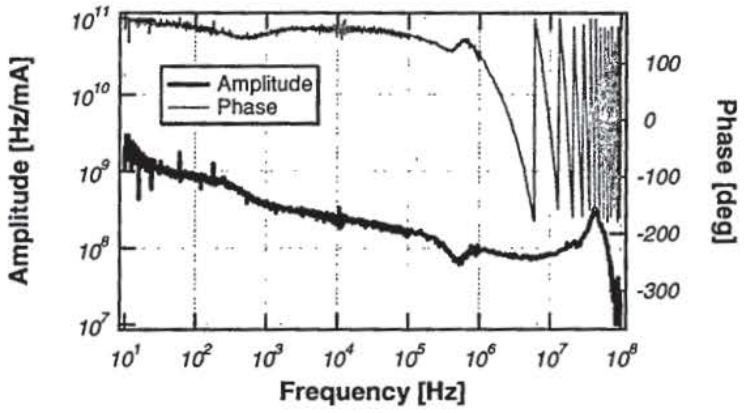

Fig. 4. Frequency tuning response of the DFB-LDs as a function of the injection current modulation frequency.

To facilitate feedback loop servo design, the DFB-LD frequency tuning response to the injection current was measured (Fig. 4). In this measurement, a fiber Michelson interferometer (MI) was used as the frequency discriminator to detect frequency variations induced by a modulation voltage applied to the injection current feedback port of the DFB-LD. The MI was auto-biased at a quadrature point using a control circuit. The delay time difference in the two arms of the MI was 3.2 nsec. The small thermal impedance in the DFB-LD package resulted in a wide tuning bandwidth of ~1 MHz. Allowing for a 30-degree phase margin for the feedback loop, this laser tuning response set an upper limit of ~800 kHz on our unity-gain loop bandwidth.

D. Master laser frequency noise measurements

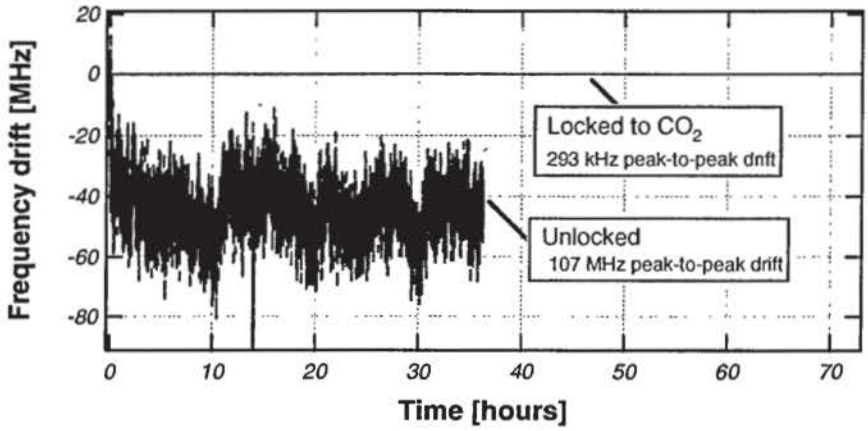

Fig. 5. Optical frequency drifts of a DFB-LD measured from the beatnote between two equivalent and independent master lasers. The frequency drifts of each one of the two lasers locked to the 1572.335-nm CO_2 line (solid red) were obtained by assuming equal and independent frequency noises from both. The unlocked frequency drifts (dashed blue) were obtained by unlocking one of the two lasers.

Since the error signal does not reflect any frequency drifts caused by error-signal shifting mechanisms (such as RAM and the noise in the detector), it is essential to measure the frequency

drift directly from the beatnote between two independent lasers (rather than from the error signal). The 10-% output tapped from each laser (external to the locking loop) was used to produce the beatnote. In order to shift the beatnote away from zero frequency for better measurement sensitivity, one laser output was frequency up-shifted by 35 MHz using a fiber-coupled acousto-optic modulator. This frequency-shifted laser output was combined with the other one using a 3-dB SM PM fiber coupler, and the combined laser output was detected by a PIN photodiode. The instantaneous frequency of the beatnote from the detector was measured by a frequency counter at a rate up to 200 Hz. As shown in Fig. 5, the frequency drift of a DFB-LD was suppressed to 293 kHz peak-to-peak (with a standard deviation of 59 kHz) at 0.8-sec averaging time over 72 hours when locked to the 1572.335-nm CO_2 line. By contrast, the frequency drift was 107 MHz over 36 hours when the laser was unlocked.

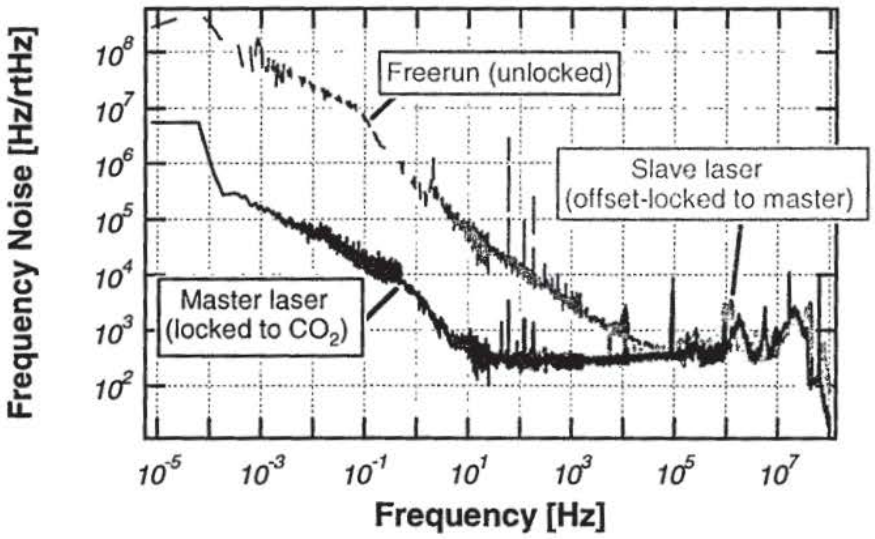

Fig. 6. DFB-LD optical frequency noise spectra measured for: 1) an unlocked laser (dashed blue); 2) a master laser absolutely locked to a CO_2 cell using the setup shown in Fig. 2 (solid red); 3) a slave laser offset locked to the master laser using the setup shown in Fig. 8 (solid gray).

Figure 6 shows measured frequency noise spectra of the DFB-LDs when locked and unlocked. For slow noise frequencies up to 100 Hz, the spectra were derived from the beatnote measured with the frequency counter (as described above). The rest of the spectra were measured with a fiber MI similar to the one used for laser frequency tuning response measurements. To suppress seismic and acoustic disturbances, the MI was mechanically stabilized by vibration-isolating stages suspended in a vacuum chamber. As seen in Fig. 6, the frequency noise of the absolutely-locked DFB-LD was suppressed within the 800 kHz unity-gain bandwidth, by a factor up to ~1000 for slow frequency noises. The fractional Allan deviation of the two absolutely-locked master DFB-LDs was measured to be $< 3\times10^{-11}$ for a gating time up to 1000 sec, as shown in Fig. 7. This stability is much higher than those obtained by using the WM technique (for example, 300~2500 times better than reported in [28]).

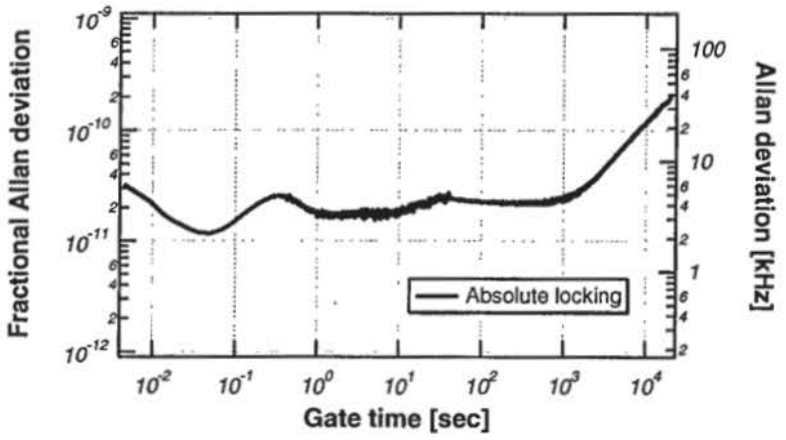

Fig. 7. The Allan deviation of the two absolutely-locked master DFB-LDs.

3. Offset frequency locking

A. Offset locking setup

In order for the slave DFB-LDs to retain the frequency stability of the master laser, the fluctuation of the frequency offset must be suppressed to a small fraction of the frequency noise of the master laser. Various offset locking techniques have been developed to lock the frequency difference between two lasers [28-32]. Our offset-locking setup, shown in Fig. 8, was based on the scheme described in [30] that appears to be most suitable to our purpose yet easy to implement with DFB-LDs.

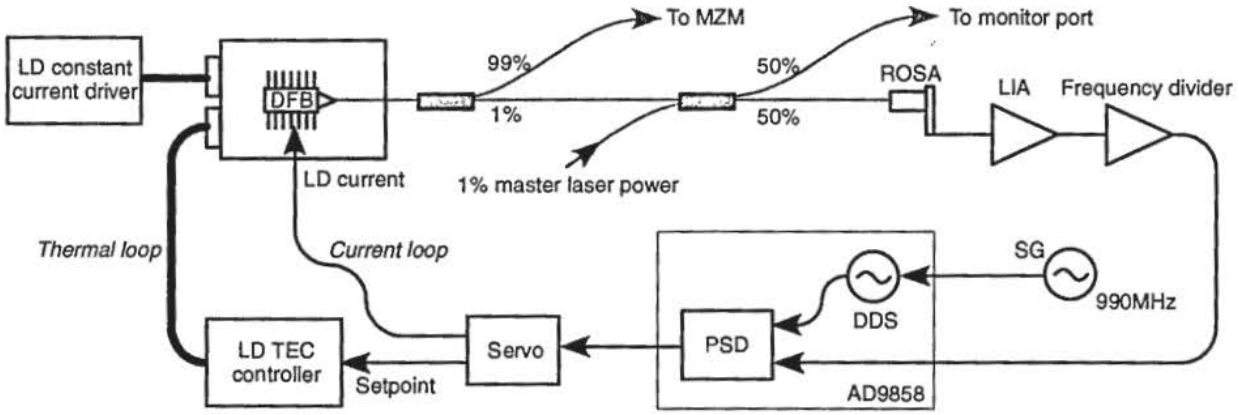

Fig. 8. Offset frequency locking setup for the slave DFB-LDs: ROSA – 10-GHz PIN-TIA detector; LIA – limiting amplifier; DDS – direct digital synthesizer; PSD – phase sensitive detector.

The four online and two offline DFB-LDs were identical to the master DFB-LD. Referring to Fig. 1, we have offset-locked two online DFB-LDs to ν_3 and ν_4 with frequency offsets of ±755.2 MHz, and two other online DFB-LDs to ν_2 and ν_5 with frequency offsets of ±2.014 GHz. The two free-running offline DFB-LDs (ν_1 and ν_6) were placed ±15.6 GHz away from the CO_2 line center.

The beatnote between each slave laser and the master is frequency-divided and then phase-locked to an RF reference signal. As shown in Fig. 8, 1 % of the slave DFB-LD power was tapped off for the offset locking and the remaining 99 % was transmitted towards its MZM. Using a SM PM fiber splitter, the 10-% light tapped from the master laser was further split into

multiple fiber outputs, each with ~1 % of the master laser power. The 1-% slave laser power was mixed with the 1-% master laser power using a 3-dB SM PM fiber coupler. The combined laser output was detected by a 10-GHz telecom receiver optical sub-assembly (ROSA) that consists of a PIN photodiode followed by an integrated TIA. The sinusoidal beatnote detected by the ROSA was amplified by a limiting amplifier (LIA) and then frequency-divided by a digital frequency divider by a factor of 8 for 755.2-MHz offset, or 16 for 2.014-GHz offset. A digital phase sensitive detector (PSD) was used to detect the phase difference between the divided beatnote and a precision electronic reference signal generated by a direct digital synthesizer (DDS), and to generate an error signal proportional to this phase difference. A commercial IC chip (AD9858, Analog Devices, Inc.) was used to provide both PSD and DDS functions. The servo sent feedback signals to and frequency-stabilized the slave DFB-LD in the same way as described for the master laser. Externally driven by a 990-MHz reference clock, the DDS output can be fast tuned with digital commands to produce the reference signal at desired frequencies, with great accuracy and flexibility. For the four online lasers, the reference signal was tuned to 94.4 MHz or 125.9 MHz for ±755.2 MHz or ±2.014 GHz offsets, respectively. The frequency divider, PSD, DDS, and servo circuits were controlled by a microcontroller, providing auto-tuning and auto-locking functions.

It should be noted that the error signal from the PSD is proportional to the integral of the laser frequency deviation, rather than to the frequency deviation itself as is the case in the master laser locking setup. This was taken into account in the servo design. We have carefully designed the servo and achieved the maximum unity-gain bandwidth of ~800 kHz for the slave laser as well. This bandwidth is sufficient for our CO_2 laser sounder system. The maximum frequency

offset can be increased to 20 GHz by replacing the PIN-TIA detector, the LIA, and the frequency divider with 20 GHz components, which are commercially available.

B. Slave laser frequency noise measurements

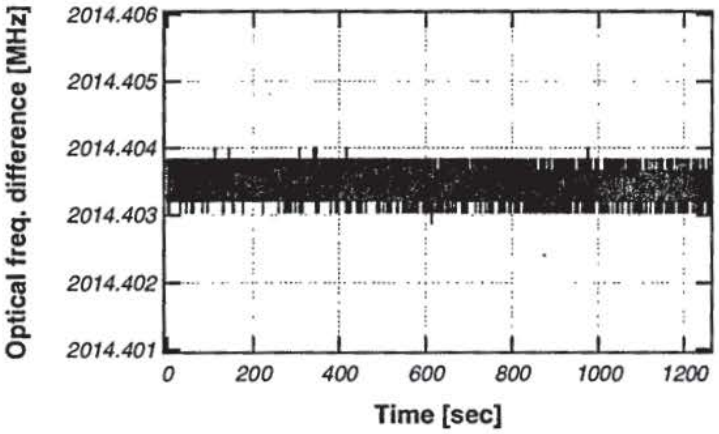

Fig. 9. Optical frequency difference between a slave DFB-LD and a maser DFB-LD when the slave was locked to the master with 2.014-GHz frequency offset using a phase locked loop shown in Fig. 8.

The frequency difference (beatnote) between the master and slave lasers was directly measured with a frequency counter at 200-Hz sampling rate and the result is shown in Fig. 9. When offset-locked, the peak-to-peak fluctuation of the frequency offset was <1 kHz, a negligible fraction of the master laser frequency drift. We further found that most of the fluctuation came from the reference signal generated by the DDS. The frequency noise spectra of offset-locked DFB-LDs were also measured in the same way as for the master laser, and were found to be essentially identical to that of the master laser (see Fig. 3). This means that a slave laser can be tuned to any wavelength across the CO_2 line with virtually identical absolute frequency stability as the master laser. Since the frequency-divided beatnote (between the master and slave lasers) was phase-

locked to the RF reference signal, no constant deviation was found between the two. This means the offset frequency locking is completely accurate without any DC error.

4. Seeder pulse-train generation

A. Setup for pulse-train generation

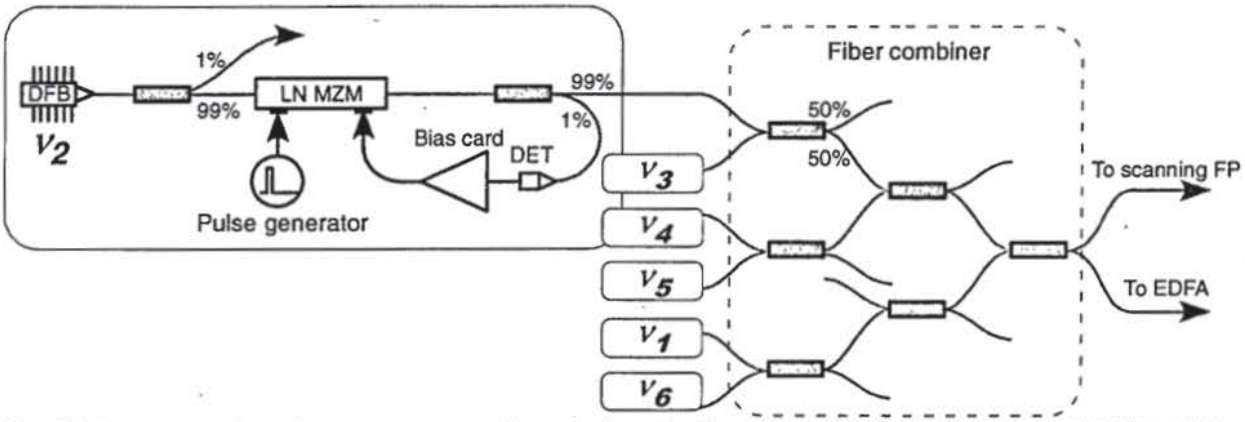

Fig. 10. Setup to produce the measurement pulse train from the 6 online and offline DFB-LDs: LN MZM – lithium-niobate Mach-Zehnder modulator; DET – detector; FP – Fabry-Perot. The fiber combiner was built from cascaded 3-dB SM PM fiber couplers.

As shown in Fig. 10, the 6 lasers (ν_1 to ν_6) were individually modulated by 6 MZMs and subsequently combined to produce the measurement pulse train. The x-cut LN MZMs (MXPE-LN-10-PD-P-P-FA-FA, Photline Technologies) have intrinsic extinction ratio (ER) > 40 dB and were auto-biased at null points and pulsed with on/off RF signals. X-cut LN MZMs were selected to minimize the optical frequency chirping during the on/off modulation. Standard MZM bias controllers typically add ~3 dB more off-state leakage and this ER penalty becomes more severe at the low pulse rate (~1 kHz) for our application. This problem was solved with customized MZM bias controllers (Mini-MBC-1B, YY Labs Inc.). For each MZM, 1-% MZM

output was tapped out and fed to the bias card that biases the MZM automatically. The on/off ER was measured to be virtually the same as the intrinsic ER, with negligible auto-bias ER penalty (< 0.6 dB) even for slow pulse rates down to 1 kHz. The ER of the MZMs changes by > 4 dB when the bias voltage changes polarity. The custom bias card permits bias polarity selection to pick the better null point. It would have been simpler to use the photodiode integrated into the MZM to feed the bias card. However, this arrangement resulted in an inferior ER, probably because the built-in detector sees the maximum light intensity (hence larger shot noise) when the MZM is biased at a null point.

The 6 MZMs were driven by one multi-channel digital delay pulse generator (Model 9518+, Quantum Composers, Inc.) that generates 1-μsec pulses at 1.25 kHz for each MZM. All 6 laser pulse trains were combined using a SM PM fiber combiner built from cascaded 3-dB SM PM couplers. A proper time delay was set in the pulse generator for each MZM, to maintain equal pulse separation of ~133 μsec in the seeder output. The on/off ER for this combined seeder pulse train was better than 38 dB.

B. Laser seeder output measurements

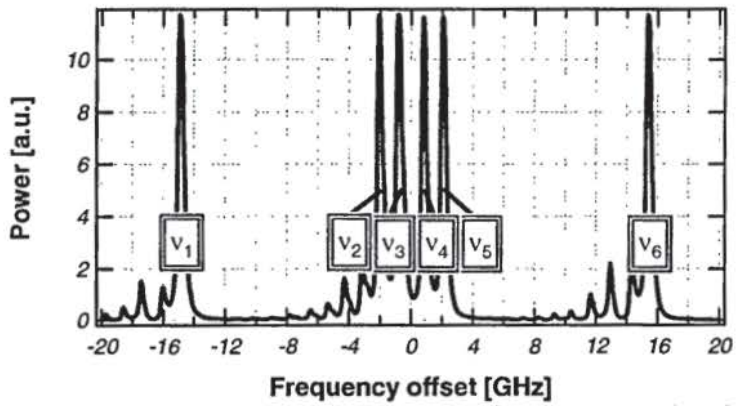

Fig. 11. Optical spectrum of the seeder output measured by a scanning Fabry-Perot interferometer. The laser seeder stepped through the 6 fixed laser frequencies across the 1572.335-nm CO_2 line centered at 0-Hz offset in this plot.

The optical spectrum of the seeder output was measured using a scanning plane-plane Fabry-Perot (FP) interferometer with ~60-GHz free spectral range. As shown in Fig. 11, frequency offsets relative to the CO_2 line center were indeed ±755.2 MHz and ±2.014 GHz for the four online DFB-LDs and ~ ±15.6 GHz for the two offline DFB-LDs. The spurious peaks in the spectrum were due to parasitic resonance in the plane-plane FP interferometer.

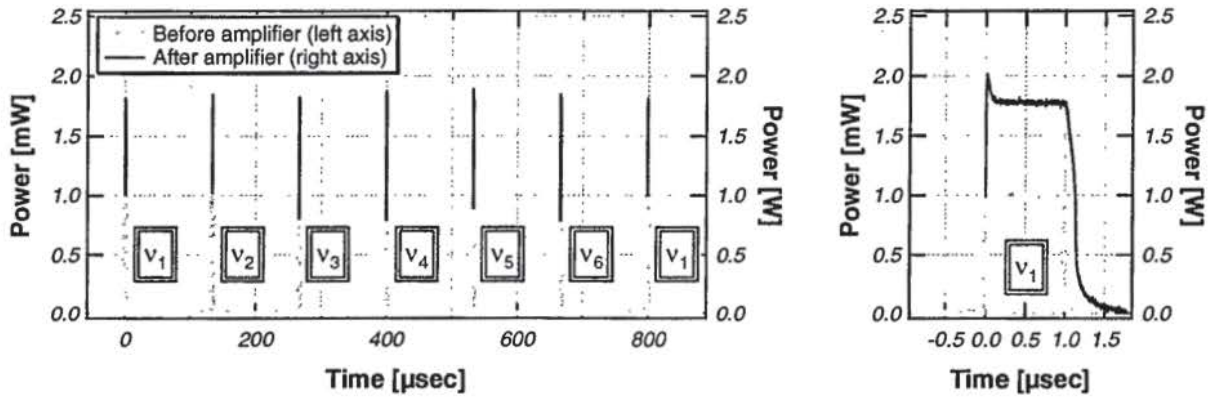

Fig. 12. Combined seeder pulse train (*left*) and pulse shapes (*right*) before and after being amplified by an EDFA preamplifier.

This combined seeder output was amplified by a SM PM EDFA pre-amplifier. Figure 12 shows pulse train waveforms measured before and after the pre-amplifier. The preamplifier output will be amplified by an EDFA power amplifier, and finally by a waveguided Erbium-doped phosphate-glass power amplifier to boost the pulse energy to ~3 mJ as required for ASCENDS measurements. Due to the narrow linewidth and long pulse duration of the laser seeder, the stimulated Brillouin scattering (SBS) in the subsequent power amplifiers becomes a major challenge. The peak power in each power amplifier is limited by the SBS threshold that is well below thresholds of other non-linear effects (such as self-phase modulation). The frequency

stability and narrow linewidth of the laser seeder will thus be well preserved at the transmitter output. Due to the gain saturation in the power amplifiers, the top-hat pulse shape of our laser seeder would be distorted at the transmitter output to have lower power at the trailing edge than the leading edge. This distortion can be counteracted by pre-distortion of the input pulse shape. This pulse pre-distortion can be accomplished by using one more LN MZM placed after the EDFA preamplifier. The on/off ER of the laser pulses can also be improved by gating the modulator to block the light between consecutive pulses, particularly the amplified spontaneous emission (ASE) from the preamplifier.

5. Discussions

A. Noise sources in absolute frequency locking

In our absolute locking setup, a sufficient laser power (> 2 dBm) was detected by the PIN detector so that the detector shot noise and the TIA noise were negligible compared to the RAM induced noise. When the detected laser power is above -6 dBm, the shot noise becomes larger than the ~8 pA/√Hz equivalent input noise of the TIA, and the sum of both noises becomes a negligible fraction of the RAM-induced noise. RAM was the predominant noise source causing slow laser frequency drifts. We further noticed that the master laser locked to the CO_2 line center exhibited a constant frequency offset from the reference line center, typically a couple of hundred kHz. This offset is attributed to the constant component of the RAM and imperfect electronic components. It should also be noted that the 1572.335-nm atmospheric CO_2 line is pressure shifted from the CO_2 cell reference line by -0.25 MHz/Torr [33]. The overall offset can

be calibrated with an external reference and corrected by shifting the offset-locking reference frequencies.

B. CO_2 cell improvements

This laser seeder was constructed with telecom fiber-optic components, except for the bulky CO_2 cell we built for lab experiments. Much more compact CO_2 cells are required for flight missions. As an improvement, we replaced the bulky cell with a compact 18-m Herriott CO_2 gas cell (Model 5612, New Focus, Inc.) and achieved essentially the same absolute locking performance as described above. The laser beam was coupled in and out of the Herriott cell through a coated, wedged optical window, to minimize MPI. The output beam was focused directly onto the PIN detector without fiber coupling, resulting in an overall cell insertion loss of ~9 dB (gas absorption excluded). Although the detected laser power was reduced by ~4 dB due to this higher cell insertion loss, there appeared to be no S/N penalty.

It would be more desirable to build all-fiber CO_2 cells using hollow-core photonic crystal fibers (HC-PCFs) for size, weight, stability, and reliability advantages [34]. However, replacing the free-space CO_2 cell with an equivalent HC-PCF CO_2 cell in our setup resulted in much larger laser frequency drifts (~6 MHz peak to peak) than obtained with the free-space cell. Nevertheless, the frequency noise spectra in both cases were comparable for noise frequencies above a few Hz. The slow frequency drifts persisted even when back reflections at both ends of the HC-PCF were suppressed and the temperature of the HC-PCF was stabilized. Such frequency drifts could not be detected by simply monitoring the error signal as described in [35], indicating a slow mechanism that shifts the error signal directly. The photonic-bandgap HC-PCFs used to build these cells exhibit an oscillatory background in the transmission spectrum due to the effect of surface modes [36]. It appears that the large frequency drifts were driven by this time-varying

background that falls on the gas absorption lines and mimics the gas absorption. This problem could be avoided by using non-bandgap based HC-PCFs, in which the coupling between the hollow-core modes and the other modes is drastically reduced [37, 38].

C. Adding more wavelength points

Recent results of our CO_2 laser sounder experiments [39, 40] indicated that more wavelength points (>10) are needed to correct for time-varying fringes in the lidar's frequency response. This makes it more difficult to limit the uncertainty of the transmitter pulse energy measurement to a small fraction of the 0.08-% total error budget. The predominant noise in the pulse energy measurement is the beatnote between the ASE in EDFAs and the laser pulses detected by the monitoring PIN photodiode [41]. The stringent pulse-energy monitoring requirement can be met in our design by limiting the fiber combiner insertion loss to < 11 dB, using low-noise EDFAs, and allowing sufficient integration time (> 10 nsec) for the monitoring PIN detector to reduce the ASE-pulse beating noise. However, our three-stage fiber combiner (shown in Fig. 10) already has ~11 dB insertion loss and can combine 8 lasers at most. Although more channels can still be combined by inserting additional EDFAs and modulators within the combiner to counteract the additional insertional losses and crosstalks, combining more lasers will significantly complicate the laser seeder design.

It would thus be highly desirable to replace the multiple online and offline DFB-LDs (and their modulators) with one precision fast tunable laser (and one modulator), to eliminate the combining loss and crosstalk. The frequency of this tunable laser needs to be accurately stepped through multiple points across the CO_2 line, as fast as ~100 μsec per step and as precise as ~0.2 MHz peak-to-peak. This would greatly simplify the seeder architecture yet enable better

performance in terms of the S/N, reliability, flexibility, power consumption, size, mass, and cost. More wavelength channels can be added without performance penalty.

We have recently started our development effort on the HC-PCF cells and the precision fast tunable lasers. We are also refining the present seeder system for field measurements. Further results will be reported as progresses are made in the future.

6. Conclusions

A fiber-based pulsed laser seeder system was developed for measurements of global CO_2 mixing ratios to 1-ppmv precision. One master DFB laser diode has been frequency-locked to the 1572.335-nm CO_2 line using a FM technique, suppressing its peak-to-peak frequency noise to 0.3 MHz at 0.8 sec averaging time over 72 hours. Slave DFB-LDs have been offset locked up to ±7 GHz away from the master laser, with virtually the same sub-MHz precision in their absolute frequencies. Over 40 dB ER has been achieved in auto-biased MZMs to modulate continuous-wave lasers into pulses. Based on these techniques, the pulsed laser seeder was built to rapidly switch among 6 fixed wavelengths across the CO_2 line. The sub-MHz frequency precision for online lasers satisfies the ASCENDS requirement.

Acknowledgements

The authors gratefully acknowledge A. Stummer at University of Toronto for sharing technical details of his laser offset-locking system through website postings. They are also indebted to Y. Yin at YY labs, Inc. for developing custom MZM bias controllers, B. Merritt and the modulator design team at JDSU Corp. for helpful discussions on the RAM in the phase modulators, J. Mao

at NASA Goddard for providing atmospheric CO_2 absorption modeling results. R. DiSilvestre at NASA Goddard machine shop and F. Kimpel at Fibertek, Inc. contributed to the construction of the laser seeder system, and the authors are appreciative of their skillful assistance. This work was supported by NASA ESTO IIP Program and NASA Goddard IRAD program.

References

1. J. R. Petit, J. Jouzel, D. Raynaud, N. I. Barkov, J.-M. Barnola, I. Basile, M. Bender, J. Chappellaz, M. Davis, G. Delaygue, M. Delmotte, V. M. Kotlyakov, M. Legrand, V. Y. Lipenkov, C. Lorius, L. PÉpin, C. Ritz, E. Saltzman, and M. Stievenard, "Climate and atmospheric history of the past 420,000 years from the Vostok ice core, Antarctica," Nature **399**, 429-436 (1999).
2. R. J. Engelen, A. S. Denning, K. R. Gurney, and G. L. Stephens, "Global observations of the carbon budget: 1. Expected satellite capabilities for emission spectroscopy in the EOS and NPOESS eras," J. Geophys. Res. **106**, 20055–20068 (2001).
3. P. J. Rayner and D. M. O'Brien, "The Utility of Remotely Sensed CO_2 Concentration Data in Surface Source Inversions," Geophys. Res. Lett. **28**, 175-178 (2001).
4. C. E. Miller, D. Crisp, P. L. DeCola, S. C. Olsen, J. T. Randerson, A. M. Michalak, A. Alkhaled, P. Rayner,D. J. Jacob, P. Suntharalingam, D. B. A. Jones, A. S. Denning, M. E. Nicholls, S. C. Doney, S. Pawson, H. Boesch, B. J. Connor, I. Y. Fung, D. O'Brien, R. J. Salawitch, S. P. Sander, B. Sen, P. Tans, G. C. Toon, P. O. Wennberg, S. C. Wofsy, Y. L. Yung, and R. M. Law, "Precision requirements for space-based Xco_2 data," J. Geophys. Res. **112**, D10314 (2007).

5. Space Studies Board, National Research Council, *Earth Science and Applications from Space: National Imperatives for the Next Decade and Beyond* (National Academies Press, 2007).

6. M. Marquis and P. Tans, "Carbon Crucible," Science **320**, 460-461 (2008).

7. Atmospheric Infrared Sounder (AIRS), http://airs.jpl.nasa.gov.

8. "Greenhouse gases observing satellite "IBUKI" (GOSAT)", http://www.jaxa.jp/projects/sat/gosat/index_e.html.

9. J. B. Abshire, H. Riris, G. Allan, X. Sun, S. R. Kawa, J. Mao, M. Stephen, E. Wilson, and M. A. Krainak, "Laser Sounder for Global Measurement of CO_2 Concentrations in the Troposphere from Space," in Laser Applications to Chemical, Security and Environmental Analysis, OSA Technical Digest (CD) (Optical Society of America, 2008), paper LMA4.

10. J. Mao and S. R. Kawa, "Sensitivity studies for space-based measurement of atmospheric total column carbon dioxide," Appl. Opt. **43**, 914-927 (2004).

11. G. Ehret, C. Kiemle, M. Wirth, A. Amediek, A. Fix, and S. Houweling, "Space-borne remote sensing of CO_2, CH_4, and N_2O by integrated path differential absorption lidar: a sensitivity analysis," Appl. Phys. B. **90**, 593-608 (2008).

12. W. C. Swann and S. L. Gilbert, "Pressure-induced shift and broadening of 1510–1540-nm acetylene wavelength calibration lines," J. Opt. Soc. Am. B **17**, 1263-1270 (2000).

13. C. S. Edwards, H. S. Margolis, G. P. Barwood, S. N. Lea, P. Gill, G. Huang, and W. R. C. Rowley, "Absolute frequency measurement of a 1.5-mm acetylene standard by use of a combined frequency chain and femtosecond comb," Opt. Lett. **29**, 566 (2004).

14. W. C. Swann and S. L. Gilbert, "Line centers, pressure shift, and pressure broadening of 1530-1560 nm hydrogen cyanide wavelength calibration lines," J. Opt. Soc. Am. B **22**, 1749-1756 (2005).

15. A. Bruner, V. Mahal, I. Kiryuschev, A. Arie, M. A. Arbore, and M. M. Fejer, "Frequency Stability at the Kilohertz Level of a Rubidium-Locked Diode Laser at 192.114 THz," Appl. Opt. **37**, 6410 (1998).

16. A. Amediek, A. Fix, M. Wirth, and G. Ehret, "Development of an OPO system at 1.57 μm for integrated path DIAL measurement of atmospheric carbon dioxide," Appl. Phys. B **92**, 295-302 (2008).

17. H. Tsuchida, T. Tako, "Limit of the frequency stability in AlGaAs semiconductor lasers," Jap. J. Appl. Phys. **22**, 1870-1875 (1983).

18. G. C. Bjorklund, "Frequency-Modulation Spectroscopy: a New Method for Measuring Weak Absorptions and Dispersions," Opt. Lett. **5**, 15-17 (1980).

19. J. L. Hall, L. Hollberg, T. Baer, and H. G. Robinson, "Optical heterodyne saturation spectroscopy," Appl. Phys. Lett. **39**, 680 (1981).

20. R. W. P. Drever, J. L. Hall, F. V. Kowalski, J. Hough, G. M. Ford, A. J. Munley, H. Ward, "Laser phase and frequency stabilization using an optical resonator," Appl. Phys. B **31**, 97-105 (1983).

21. E. A. Whittaker, M. Gehrtz, and G. C. Bjorklund, "Residual Amplitude Modulation in Laser Electro-Optic Phase Modulation," J. Opt. Soc. Am. B **2**, 1320-1326 (1985).

22. N. C. Wong and J. L. Hall, "Servo control of amplitude modulation in frequency-modulation spectroscopy: demonstration of shot-noise-limited detection," J. Opt. Soc. Am. B **2**, 1527-1533 (1985).

23. F. Bertinetto, P. Gambini, R. Lano, and M. Puleo, "Frequency stabilization of DFB laser diodes to the P(3) line of acetylene at 1.52688 μm by external phase modulation," in Frequency Stabilized Lasers and Their Applications, Y. C. Chung, ed., Proc. SPIE 1837, 154–163 (1992).

24. M. W. Phillips, J. Ranson, G. D. Spiers, and R. T. Menzies, "Development of a coherent laser transceiver for the NASA CO_2 laser absorption spectrometer instrument," in Conference on Lasers and Electro-Optics/International Quantum Electronics Conference and Photonic Applications Systems Technologies, Technical Digest (CD) (Optical Society of America, 2004), paper CMDD2.

25. G. J. Koch, J. Y. Beyon, F. Gibert, B. W. Barnes, S. Ismail, M. Petros, P. J. Petzar, J. Yu, E. A. Modlin, K. J. Davis, and U. N. Singh, "Side-line tunable laser transmitter for differential absorption lidar measurements of CO_2: design and application to atmospheric measurements," Appl. Opt. **47**, 944-956 (2008).

26. L. Hilico, D. Touahri, F. Nez, and A. Clairon, "Narrow-line, low-amplitude noise semiconductor laser oscillator in the 780 nm range," Rev. Sci. Instrum. **65**, 3628-3633 (1994).

27. I. A. Ramsay and J. J. Degnan, "A Ray Analysis of Optical Resonators Formed by Two Spherical Mirrors," Appl. Opt. **9**, 385 (1970).

28. R. Matthey, S. Schilt, D. Werner, C. Affolderbach, L. Thévenaz, and G. Mileti, "Diode laser frequency stabilisation for water-vapour differential absorption sensing," Appl. Phys. B **85**, 477-485 (2006).

29. S. Schilt, R. Matthey, D. Kauffmann-Werner, C. Affolderbach, G. Mileti, and L. Thévenaz, "Laser offset-frequency locking up to 20 GHz using a low-frequency electrical filter technique," Appl. Opt. **47**, 4336-4344 (2008).

30. A. Stummer, ""Chroma-Matic" Laser Tuning," http://www.physics.utoronto.ca/~astummer/pub/mirror/Projects/Archives/Laser%20Tuning/Laser%20Tuning.html

31. R. T. Ramos and A. J. Seeds, "Fast heterodyne optical phase-lock loop using double quantum well laser diodes," Electron. Lett. **28**, 82–83 (1992).

32. U. Schünemann, H. Engler, R. Grimm, M. Weidemüller, and M. Zielonkowski, "Simple scheme for tunable frequency offset locking of two lasers," Rev. Sci. Instrum. **70**, 242-243 (1999).

33. D. Sakaizawa, C. Nagasawa, T. Nagai, M. Abo, Y. Shibata, and M. Nakazato, "Measurement of pressure-induced broadening and shift coefficients of carbon dioxide absorption lines around 1.6 μm for using differential absorption lidar," Jap. J. Appl. Phys. **47**, 325-328 (2008).

34. F. Benabid, F. Couny, J. C. Knight, T. A. Birks, and P. S. J. Russell, "Compact, stable and efficient all-fibre gas cells using hollow-core photonic crystal fibres," Nature **434**, 488-491 (2005).

35. P. Meras Jr., I. Y. Poberezhskiy, D. H. Chang, J. Levin, and G. D. Spiers, "Laser frequency stabilization for coherent lidar applications using novel all-fiber gas reference cell fabrication technique," presented at 24th International Laser Radar Conference, Boulder, Colorado, June 23, (2008).

36. C. M. Smith, N. Venkataraman, M. T. Gallagher, D. Müller, J. A. West, N. F. Borrelli, D. C. Allan, and K. W. Koch, "Low-loss hollow-core silica/air photonic bandgap fibre," Nature **424**, 657-659 (2003).

37. F. Couny, F. Benabid, and P. S. Light, "Large-pitch kagome-structured hollow-core photonic crystal fiber," Opt. Lett. **31**, 3574–3576 (2006).

38. K. Knabe, S. Wu, J. Lim, K.A. Tillman, P. S. Light, F. Couny, N. Wheeler, R. Thapa, A. M. Jones, J. W. Nicholson, B. R. Washburn, F. Benabid, and K. L. Corwin, "10 kHz accuracy of an optical frequency reference based on $^{12}C_2H_2$-filled large-core kagome photonic crystal fibers," Opt. Express **17**, 16017-16026 (2009).

39. G. R. Allan, H. Riris, J. B. Abshire, X. Sun, E. Wilson, J. F. Burris, and M. A. Krainak, "Laser sounder for active remote sensing measurements of CO2 concentrations," IEEE Aerospace Conference 2008, Big Sky, Montana, pages: 1-7, ISSN: 1095-323X, ISBN: 978-1-4244-1487-1.

40. J. Abshire, H. Riris, W. Hasselbrack, G. R. Allan, C. J. Weaver, and J. Mao, "Airborne measurements of CO_2 column absorption using a pulsed wavelength-scanned laser sounder instrument," in Conference on Lasers and Electro-Optics/International Quantum Electronics Conference, OSA Technical Digest (CD) (Optical Society of America, 2009), paper CFU2.

41. P. C. Becker, N. A. Olsson, and J. R. Simpson, *Erbium-doped fiber amplifiers: fundamentals and technology* (Academic, 1999).